Detecting nonstationarity and state transitions in a time series

J. B. Gao*
Department of Electrical Engineering, University of California, Los Angeles, California 90095
(Received 15 March 2000; revised manuscript received 18 December 2000; published 11 May 2001)

One cause of complexity in a time series may be due to nonstationarity and transience. In this paper, we analyze the nonstationarity and transience in a number of dynamical systems. We find that the nonstationarity in the metastable chaotic Lorenz system is due to nonrecurrence. The latter determines a lack of fractal structure in the signal. In $1/f^{\alpha}$ noise, we find that the associated correlation dimension are local graph dimensions calculated from sojourn points. We also design a transient Lorenz system with a slowly oscillating controlling parameter, and a transient Rossler system with a slowly linearly increasing parameter, with parameter ranges covering a sequence of chaotic dynamics with increased phase incoherence. State transitions, from periodic to chaotic, and vice versa, are identified, together with different facets of nonstationarity in each phase.

DOI: 10.1103/PhysRevE.63.0462XX PACS number(s): 05.45.Tp; 02.50.Fz

I. INTRODUCTION

Almost all existing linear and nonlinear time series analysis techniques assume that the time series under investigation is stationary. However, many time series occurring in geophysics, physiology, finance, etc., are nonstationary. The nonstationarity may be attributed to slow drift of the system's parameters during a measurement period, a changing environment, etc. The existence of nonstationarity can cause the interpretation of the results of many data analysis methods, especially those based on chaos theory, to be problematic. For example, it was once thought that an estimated positive Lyapunov exponent or entropy, or a finite noninteger correlation dimension would suffice to indicate that the time series is chaotic. If this were true, then one would have to conclude that $1/f^{\alpha}$ noise, $1<\alpha<3$, is chaotic, since it produces a positive K_2 entropy [1] and a finite noninteger correlation dimension, $D=2/(\alpha-1)$ [2]. We now understand that such a conclusion is incorrect, since the $1/f^{\alpha}$ process is just noise. Hence, simple and efficient methods capable of detecting nonstationarity in a time series would be valuable to researchers from a diversity of fields.

This subject has attracted much attention recently. Proposed methods include recurrence plots [3] and recurrence quantification analysis [4], space-time separation plots [5], and their associated probability distributions [6], metadynamical recurrence plot [7], a statistical test using the information of the distribution of points in the reconstructed phase space [8], a cross-correlation sum analysis [9], and nonlinear cross prediction analysis [10]. Most of these methods are based on quantifying certain aspects of the nearest neighbors in phase space. It has been recently shown [11] that the nearest neighbors in phase space can be broken down into true recurrence points and sojourn points. Accordingly, these two types of recurrence points define two types of recurrence times. Two convenient algorithms for detecting transience and nonstationarity in a time series have been developed based on the second type of recurrence times. In this paper, we shall first more fully explore the capabilities (and possibly limitations) of those methods by applying them to a number of interesting nonstationary time series, namely, the metastable chaotic Lorenz system, $1/f^{\alpha}$ noise, a transient Lorenz system with a slowly oscillating controlling parameter, and a transient Rossler system with a slowly linearly increasing parameter, with parameter ranges covering a sequence of chaotic dynamics with increased phase incoherence [12]. We shall show that nonstationarity in the metastable chaotic Lorenz system and $1/f^{\alpha}$ noise is due to nonrecurrence, and explore the consequences of nonrecurrence. In the transient Lorenz and Rossler system, we shall show how the method identifies state transitions, from periodic to chaotic, and vice versa, and characteristics of nonstationarity in each phase.

The remainder of the paper is organized as follows. In Sec. II, we briefly review recurrence time statistics for deterministic chaos in dissipative systems and the two algorithms for the detection of nonstationarity and bifurcations. In Sec. III, we detect nonstationarity in the metastable chaotic Lorenz system and in $1/f^{\alpha}$ noise. In Sec. IV, we design the transient Lorenz and Rossler systems to simulate the situation common in experiments where one wishes to zero in on bifurcations, and analyze various facets of nonstationarity in these systems. For simulating the scenario of scanning a wide range of parameters, we refer to the transient logistic map [4,11] and the transient Lorenz system [13,14]. These four systems provide easy-to-implement examples for detecting state transitions in dynamical systems. Finally, we give conclusions in Sec. V.

II. RECURRENCE TIME STATISTICS FOR DISSIPATIVE CHAOTIC SYSTEMS AND DETECTION OF CHANGES IN DYNAMICS

Most methods for detection of nonstationarity are based on quantifying features of nearest neighbors. The nearest neighbors are also called Poincare recurrence points, and are further divided into two classes [11], with two types of recurrence times.

Given a scalar time series $\{x(i), i=1,2,...\}$, we first construct vectors of the form [15]: $X_i=[\{x(i),x(i+L),\ldots,x[i$

*Email address: jbgao@ee.ucla.edu

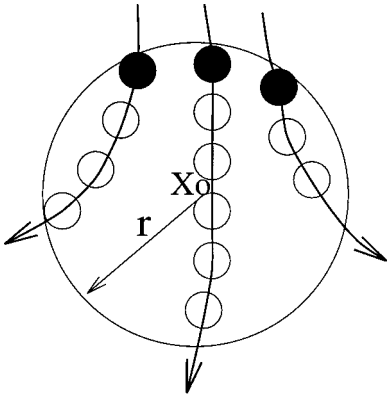

FIG. 1. A schematic showing the recurrence points of the second type (solid circles) and the sojourn points (open circles) in $B_r(X_0)$.

$+(m-1)L]\}]$, with m being the embedding dimension and L the delay time. $\{X_i,\ i=1,2,...,N\}$ then represents certain trajectory in a m-dimensional space. In this paper, we shall always normalize the time series into the unit interval [0, 1] before subsequent analysis. Next, we arbitrarily choose a reference point X_0 on the reconstructed trajectory, and consider recurrences to its neighborhood of radius r: $B_r(X_0)=\{X:\|X-X_0\|\leqslant r\}$. The subset of the trajectory that belongs to $B_r(X_0)$ is denoted by $S_1=\{X_{t_1},X_{t_2},\ldots,X_{t_i}\ldots\}$. The elements of the set S_1 are the Poincare recurrence points. Using S_1, we define the Poincare recurrence time as the element of $\{T_1(i)=t_{i+1}-t_i,\ i=1,2,...\}$. For later convenience, we call the elements of $\{T_1(i)\}$ the recurrence times of the first type.

Sometimes we may have $T_1(i)=1$ (for continuous-time systems, this means 1 unit of sampling time), for some i. This corresponds to both X_{t_i} and X_{t_i+1} belonging to S_1. For deterministic continuous-time systems with fixed (small) sampling time, if the radius r of $B_r(X_0)$ is not too small, then we can have a sequence such as $X_{t_i},X_{t_i+1},\ldots,X_{t_i+k}$ belonging to S_1, with $k\gg 1$. This is shown schematically in Fig. 1. We call the points $X_{t_i+1},\ldots,X_{t_i+k}$ (excluding X_{t_i}) ''sojourn points.'' When $k\gg 1$, each such sequence of points effectively represents a one-dimensional (1D) set. For maps or continuous-time systems with small r, the number of sojourn points are negligible. Hence, sojourn points form a 0D (empty or almost empty) set. We now remove these points from S_1 and denote the remaining points of S_1 by $S_2=\{X_{t_1'},X_{t_2'},\ldots,X_{t_i'},\ldots\}$, which in turn define a time sequence $\{T_2(i)=t_{i+1}'-t_i',\ i=1,2,...\}$. We call the elements of S_2 recurrence points of the second type, and $T_2(i)$ recurrence times of the second type.

For dissipative chaotic systems, we have shown that with fixed r, the distribution of $\{T_2(i)\}$ is exponential, due to the memoryless property of a chaotic system, and the mean of $T_1(i)$ and $T_2(i)$ are both related to the information dimension d_1 of the attractor by simple scaling laws [11],

$$\overline{T}_1(r)\sim r^{-d_1} \tag{1}$$

and

$$\overline{T}_2(r)\sim r^{-d_1'} \tag{2}$$

with $d_1'=d_1$ for discrete maps and continuous-time systems with small r (when the sojourn points form a 0D set), and $d_1'=d_1-1$ for continuous-time systems with large r (when the sojourn points form a 1D set). For a periodic signal, $T_2(i)$ simply gives an estimation of the periodicity of the signal.

Based on an observation that, due to nonstationarity, successive recurrence times of the second type will, on average, be changing with time, we have designed two ways [11] of detecting nonstationarity and state transitions:

Algorithm 1: Partition a long-time series into (overlapping or nonoverlapping) blocks of data sets of short length k, and compute $\overline{T}_2(r)$ for each data subset. The length of the subset is chosen to be short enough so that nonstationarity is not a problem for the subset. At the same time, the subset is long enough so that $\overline{T}_2(r)$ can be reliably estimated. As a rule of thumb, we recommend that the subset contains a few cycles of oscillation, if the motion is oscillatory. One may also want to choose a new length for the subset, such as $2k$ or $k/2$, and check whether the new result remains similar to that when the length of the subset is k. Usually, overlapping blocks are preferred so that bifurcation can be more accurately located. To save computation, however, we do not recommend maximal overlapping (i.e., when adjacent data subsets differ by only one point). For nonstationary and transient time series, we expect that $\overline{T}_2(r)$ will be different for different blocks of data subsets. This algorithm is best suited for the detection of state transitions in a time series (such as from chaotic to periodic, or vice versa), since $\overline{T}_2(r)$ simply estimates the periodicity of a periodic signal.

Algorithm 2: With fixed r, compute $T_2(j)$ for all the reference points in the entire dataset, where j denotes the jth return to the reference point. Nonstationarity is seen when $T_2(j)$ varies with j. Since a given region in the phase space may be visited by a given trajectory more often than other regions, to remove this dependence of visiting frequency on the phase-space location, we perform the following normalization. Let the reference point be X_0, and $T_2(j)[B_r(X_0)]$, $j=1,2,...,N_0$, be successive recurrences to $B_r(X_0)$. We normalize $T_2(j)[B_r(X_0)]$, $j=1,2,...,N_0$, by its mean. This procedure is applied to all the reference points. Next, we group the normalized $T_2(j)$ together according to j, $\{T_2(j)(X_i),\ i=0,1,2,...\}$, and compute the mean of each group, $\overline{T}_2(j)$. For nonstationary time series, $\overline{T}_2(j)$ will vary with j, while for stationary time series, $\overline{T}_2(j)$ will have an almost constant value of 1.

The classification of recurrence points and times into two types enables us to gain new insights into the structures of a recurrence plot (RP) [3,14], and to design new ways of quantifying a RP [14]. Recall that a RP is an $N\times N$ array in which a dot is placed at (i,j) whenever a point X_i on the trajectory is close to another point X_j. Hence it is clear that sojourn points will trace out a short vertical (by symmetry, also horizontal) line segment. Collection of sojourn points, hence, gives rise to squarelike textures (or blocks) in a RP. In Sec.

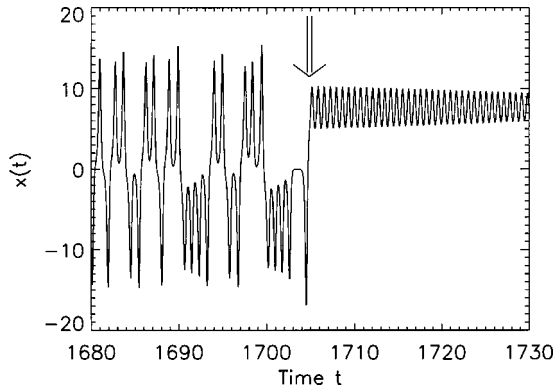

FIG. 2. An example of metastable Lorenz chaotic signal. An arrow is drawn to separate the metastable and the decaying parts of the signal.

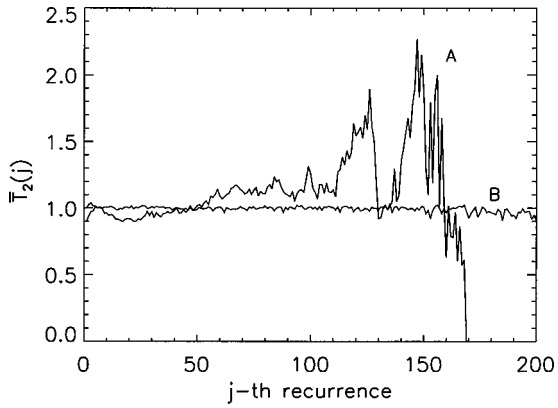

FIG. 3. Variation of $\overline{T}_2(j)$ with j for a metastable chaotic signal (curve A) and the chaotic signal (curve B). The scale r used to generate the figure is 2^{-4}. Embedding parameters are $m=4$ and $L=3$. 25 000 points are used in the calculation.

III B, we shall show that a RP for $1/f^{\alpha}$ noise typically exhibits such squarelike textures.

III. DETECTION OF NONSTATIONARITY

In this section, we apply Algorithm 2 described in the last section to detect nonstationarity in the metastable chaotic Lorenz system and in $1/f^{\alpha}$ noise.

A. Nonstationarity in the metastable chaotic Lorenz system

Some chaotic systems are found to exhibit an interesting phenomenon called metastable chaos [16], or chaotic transient [17]. Consider the Lorenz system:

$$dx/dt=-10(x-y), \quad dy/dt=-xz+Rx-y,$$

$$dz/dt=xy-8z/3. \tag{3}$$

For $R<1$, the system has a stable solution at (0, 0, 0). For $R>1$, there are three critical points, (0, 0, 0), $(a,a,R-1)$, and $(-a,-a,R-1)$, where $a=[8/3(R-1)]^{1/2}$. For R between 1 and $R_2\approx 24.74$, the two nonzero solutions are stable and attracting, and for $R>R_2$, all three critical points are unstable, and the solution is chaotic. In a range of $R_1 \approx 24.06<R<R_2$, it is observed that some trajectories tend towards the strange attractor asymptotically, while others tend asymptotically towards the stable attracting points. The former trajectories oscillate irregularly without ever settling down. Such solutions are known as ''sustained chaos'' [16].

At $R=R_0\approx 13.926$, a transition occurs [18]. Immediately above R_0 there is an ''exceptional'' set (i.e., a set with measure zero) of chaotic orbits that oscillate forever. This chaotic set is unstable for R between R_0 and R_1. Its existence, however, affects what is observed in numerical investigations, especially for R just below R_1, since the ''decay time'' for orbits near this chaotic set is very long. These predecaying trajectories are called ''metastable chaos.'' An example for $R=23.5$ is shown in Fig. 2, where we observe that the metastable chaotic oscillations last more than 1700 natural time units. With a sampling time $\delta t=0.06$, this amounts to having a time series almost as long as 3×10^4 points for the metastable chaos. We observe that visually metastable chaotic signals are quite stationary. Using some criteria for chaos such as phase diagrams and power spectra, we might classify such metastable chaotic signals as genuine chaotic signals. We apply our tests of stationarity to see whether the metastable chaos is stationary and whether it is really the same as the conventional chaos.

We have generated 6 very long metastable chaotic time series for $R=23.5$ using 6 different initial conditions. For each time series, we retain only the middle 25 000 points with sampling time $\delta t=0.06$. We apply our Algorithm 2 to analyze these time series. A typical $\overline{T}_2(j)$ vs j curve is shown in Fig. 3 as curve A. As a comparison, the result for a true chaotic time series corresponding to $R=28$ is also shown as curve B. For the true chaotic signal, we observe that $\overline{T}_2(j)$ assumes more or less a constant value of 1, as expected. However, for the metastable chaotic signal, $\overline{T}_2(j)$ varies considerably with j. This indicates that dynamically, the metastable chaos is nonstationary, though visually it appears quite stationary. While at first sight this result might not be as expected, on a second thought, one is compelled to accept it, since the variations in the time series considered here is ultimately finite (i.e., it eventually decays to a stable fixed point).

True chaotic attractors are often fractals. The fractality is caused by incessant stretching due to exponential separation of nearby trajectories, and folding due to recurrence. Hence, we surmise that nonrecurrence implies a lack of genuine fractal structure in the metastable chaotic signals studied here. To test this hypothesis, we compute the correlation dimension of the signal using the Grassberger-Procaccia algorithm [19]. Two typical results are shown in Fig. 4, where the solid lines A_1 and A_2 are computed using two different metastable chaotic data sets. Four other data sets give results similar to either A_1 or A_2. For comparison, the curve for the chaotic signal at $R=28$ is shown as the dashed curve in Fig. 4. We observe that for metastable chaotic signals, whenever the $d\log_{10}C(r)$ vs $d\log_{10}r$ curve has an appreciable plateau (with a suitably chosen delay time L), the plateau either settles at a value of 2, or the curve does not have a plateau.

While it is unrealistic to check whether all metastable

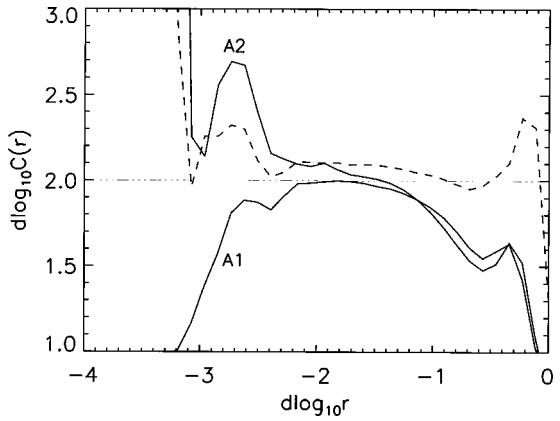

FIG. 4. Correlation dimension calculations for two metastable chaotic signals (solid lines with $m=4$ and $L=9$ and denoted as $A1$ and $A2$) and a true chaotic signal (dashed line with $m=4$ and $L=7$).

chaotic signals are nonfractals, we can conjecture that whenever a metastable chaotic signal is nonrecurrent for a number of different scales, it lacks a genuine fractal structure. Furthermore, we surmise that even though the Grassberger-Procaccia algorithm gives an appreciable plateau for some metastable chaotic signals (especially for R just below R_1), the plateau, which necessarily excludes those scales that correspond to the signals to be dynamically nonrecurrent, would be so narrow that it would be destroyed by a tiny amount of noise.

B. Nonstationarity in $1/f^{\alpha}$ noise

$1/f^{\alpha}$ noise is ubiquitous in nature and in man-made systems [20,21]. Using $1/f^{\alpha}$ noise as an example, it has been demonstrated that the correlation dimension and the K_2 entropy measures alone cannot be used to distinguish between deterministic chaos and noise [1,2]. In this section, we show that $1/f^{\alpha}$ noise is nonstationary, and that the estimated correlation dimension is simply the local graph dimension of the trajectory corresponding to the sojourn points.

$1/f^{\alpha}$ noise can be obtained through its Fourier representation [1,2], i.e., by

$$x(t_i)=\sum_{k=1}^{N/2} A(\omega_k)\cos(\omega_k t_i+\phi_k), \quad i,\ldots,N,$$

$$A^2(\omega_k)\propto \omega_k^{-\alpha}, \tag{4}$$

where $\omega_k=2\pi k/N\Delta t$ and the ϕ_k are random uncorrelated phases. We generate a number of realizations of such processes corresponding to different values of α. Each realization is 32 768 points long. To remove possible edge effects, we analyze only the middle 25 000 points. Figure 5 shows a typical $\overline{T}_2(j)$ vs j curve (corresponding to $\alpha=1.5$). We observe that $\overline{T}_2(j)$ varies considerably with j, indicating that the process is not recurrent, and is thus dynamically nonstationary.

Comparing Fig. 5 and Fig. 3 curve A's, we find that the variation of $\overline{T}_2(j)$ with j is less significant for $1/f^{\alpha}$ noise than

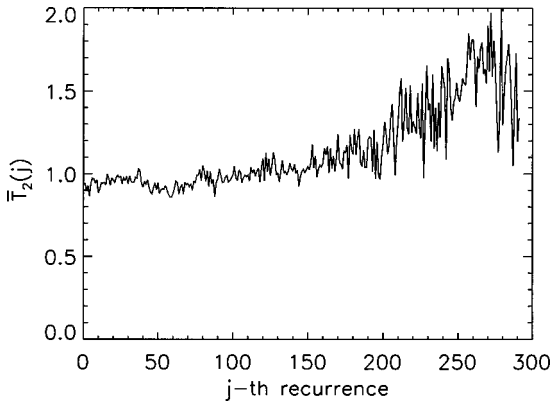

FIG. 5. Variation of $\overline{T}_2(j)$ with j. The scale r used to generate the figure is 2^{-4}. Embedding parameters are $m=6$ and $L=1$. 25 000 points are used in the calculation.

for the metastable chaotic signal. In some sense, this indicates that the $1/f^{\alpha}$ noise is less nonrecurrent on finite scales. This results in an appreciable plateau when the Grassberger-Procaccia algorithm is applied to such processes. We should note, however, that the feature of being less nonrecurrent for $1/f^{\alpha}$ noise is scale dependent. When a smaller ball of radius r is used to define neighborhoods, then $1/f^{\alpha}$ noise is more nonrecurrent.

The nonrecurrent nature of $1/f^{\alpha}$ noise can be better appreciated by computing a RP. Figure 6 shows an example. We observe that away from the main diagonal, the plot is basically blank, indicating lack of recurrence for the signal. Were a smaller r for the ball used, then the plot would be almost completely blank except just near the main diagonal. The RP shown in Fig. 6 is simply a result of the finiteness of the size for the ball. This cutoff scale corresponds to the ''knee'' observed in the dimension calculation of such processes [2]. We also observe that the structure of the RP is basically squarelike, indicating that the majority of the Poincare recurrence points are just sojourn points. Modifying Fig. 1, we can obtain a schematic shown in Fig. 7, showing that when-

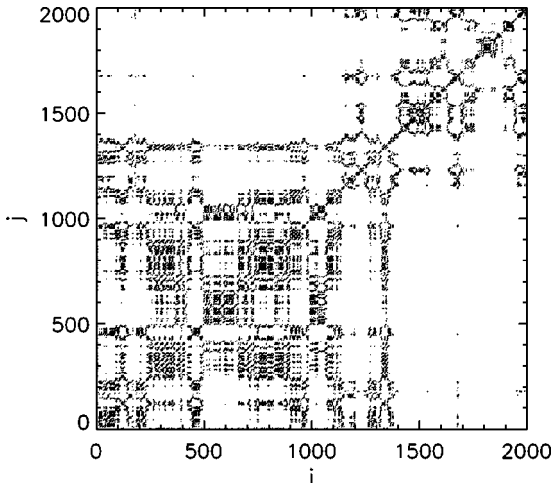

FIG. 6. A recurrence plot for a realization of $1/f^{\alpha}$ noise with $\alpha=1.5$. The embedding parameters are $m=6$ and $L=1$. The scale r used is 2^{-4}.

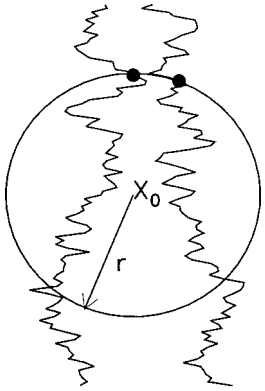

FIG. 7. A schematic showing the recurrence points of the second type (solid circles) and the sojourn points (irregular curves) in $B_r(X_0)$ for $1/f^{\alpha}$ noise.

ever a ''recurrence'' occurs, the sequence of sojourn points is fairly long, due to finiteness of the size of the ball. Hence, what the Grassberger-Procaccia algorithm estimates is the fractal dimension of such an irregular trajectory. Being able to easily estimate the key parameter for $1/f^{\alpha}$ noise should be considered a merit of the Grassberger-Procaccia algorithm.

An implication of the above results is that if an efficient algorithm for the computation of the information dimension can be developed based on Eq. (2), then a dimension calculation may suffice to indicate whether a signal is chaotic or not. By efficient we mean that the size of the data set used for this purpose should be not much larger than that needed for the Grassberger-Procaccia algorithm. This is left to future work.

We also note that if one finds the signal under study is nonstationary and belongs to $1/f^{\alpha}$ noise, the next step in the analysis of the time series may be to conduct multifractal analysis of the signal, to determine whether the signal is mono- or multifractal, and how intermittent the signal is. See Ref. [22] for an introductory account of multifractals (structure function technique and singular measures).

IV. DETECTION OF BIFURCATIONS

In this section, we design the transient Lorenz system with an oscillating parameter and the transient Rossler system with a slowly linearly increasing parameter, and study state transitions in these systems using our Algorithm 1. These systems are specifically designed to simulate a situation common in experiments where one wishes to zero in on bifurcations.

A. State transitions in the Lorenz system

Following Trulla *et al.* [4], Iwanski and Bradley designed a transient Lorenz system. The system is obtained by integrating Eq. (3) with a time step of 0.01 and incrementing the parameter R from 28.0 to 268.0 by 0.002 at each integration step. The stationary Lorenz system (corresponding to fixed R) has periodic windows at $99.524<R<100.795$, $145<R<166$, and $R>214.4$. This system has been carefully studied using our Algorithm 1 [14]. It is shown that the method

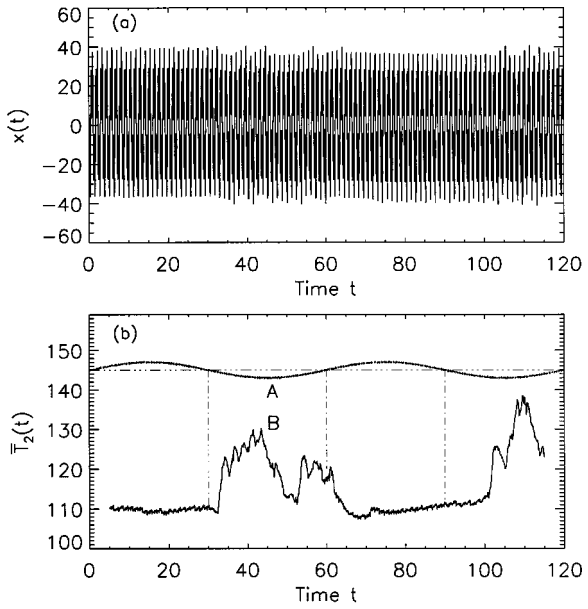

FIG. 8. (a) the transient Lorentz signal; (b) Parameter variation (curve *A*) and variation of $\overline{T}_2(r)$ with time. The embedding parameters are $m=3$ and $L=10$. The scale r used is 2^{-4}.

correctly locates the bifurcation points, and also offers a way of explaining why sometimes there are false indications of bifurcations.

Sometimes an experimentalist is most interested in locating a bifurcation point for a controlling parameter. This experimentalist would like to fix the parameter just before and after that bifurcation point, yet is unable to, due to fluctuations in the equipment and environment. The parameter sometimes becomes larger than the bifurcation point, sometimes smaller; overall, it more or less oscillates. This picture suggests that we design a transient Lorenz system in this way: integrate the Lorenz system of Eq. (3) with a fourth-order Runge-Kutta method and a timestep of 0.01, with the parameter $R(i)$ at step i being

$$R(i)=145+2\sin(2\pi i/6000)+\eta(i), \tag{5}$$

where $\eta(i)$ is an uncorrelated Gaussian noise with zero mean and standard deviation 0.05. A time series of length 12 001 points thus obtained is shown in Fig. 8(a). We observe that visually the time series is quite stationary, since the amplitude of the signal is more or less a constant. In the time interval considered, the parameter exactly oscillates two cycles, as shown in Fig. 8(b) curve A. Note the curve is blurred due to a random fluctuation.

One might expect that bifurcations occur at time instants 30, 60, and 90. This occurs if one integrates Eq. (3) with a fixed R. Re-examining Fig. 8(a), we notice that if there are transitions, then those transitions occur later than the time instants of 30, 60, and 90. This implies that transitioning from an oscillatory phase to a chaotic phase, and vice versa, requires time. To correctly locate the transition points, we compute $\overline{T}_2(r)$ on time series data within episodic windows consisting of 1000 consecutive points. Sequential windows are shifted by 10 points (thus overlapping by 990 points),

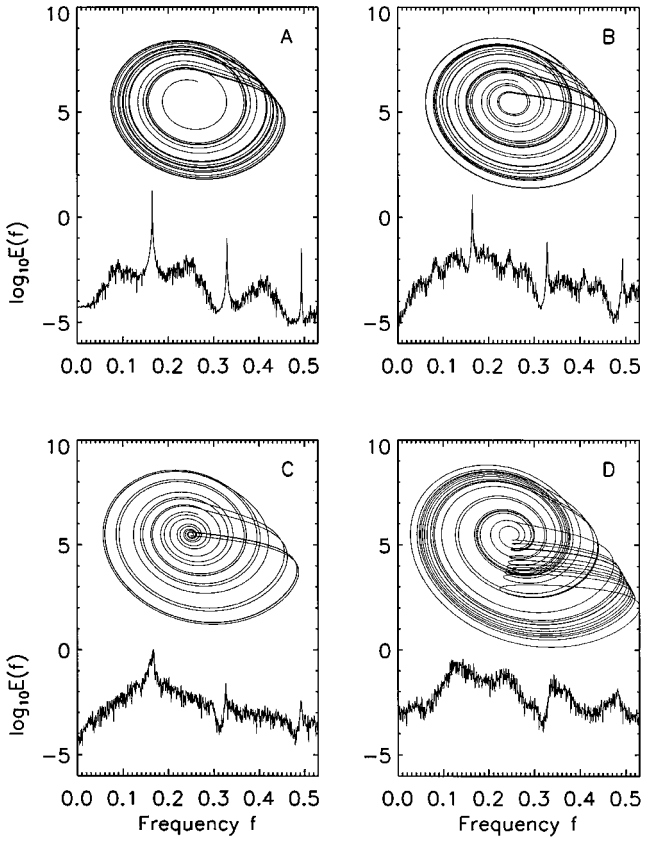

FIG. 9. Phase diagrams and power spectra for Rossler attractors. *A*, *B*, *C*, and *D* denote parameter values of $a=0.15$, 0.18, 0.21, and 0.30, respectively.

giving a total of 1101 values for $\overline{T_2}(r)$. Figure 8(b) curve *B* shows the variation of $\overline{T_2}(r)$ vs time. We observe several interesting features: the variation of $\overline{T_2}(r)$ roughly consists of two cycles, corresponding to the two cycles of the parameter variation; the time of transitions occur later than time instants of 30, 60, and 90. Due to nonstationarity, neither the two chaotic nor the two oscillatory phases are identical; inside each chaotic phase, there are wide variations, and variations inside the oscillatory phase, though much smaller, are still appreciable, indicating nonstationarity of the signal.

Note that these results are quite robust with respect to changes in the embedding parameters, the size of the ball, and the length of the data subset.

B. State transitions in the Rossler system

The Rossler system takes the form [23]:

$$dx/dt=-(y+z), \quad dy/dt=x+ay, \quad dz/dt=b+z(x-c). \tag{6}$$

The x and y equations are equivalent to those of a linear damped harmonic oscillator. All the nonlinearity comes from the $x-z$ term in the third equation. Following Farmer *et al.* [12], we choose $b=0.4$ and $c=8.5$. Four chaotic attractors corresponding to $a=0.15$, 0.18, 0.21, and 0.30 are shown in Figs. 9(a)–9(d), respectively, together with their power spectral densities (PSD), $E(f)$. [See also Ref. [12] for phase diagrams and PSD's for attractors corresponding to $a=0.17$, 0.19, and 0.20]. The attractor corresponding to $a=0.15$ has a repeller near the origin, and is usually called the simple Rossler attractor. We notice that as the parameter a is varied the attractor approaches the repeller [Fig. 9(b)] until it encompasses it [Fig. 9(c)]. The attractor rolls up around the repeller, developing a structure that has been called ''the funnel'' [Fig. 9(b)–9(d)]. As seen from the power spectrum, the simple Rossler attractor contains a sharp periodic motion superimposed on otherwise chaotic behavior. This is called phase coherence [12]. As the funnel develops more turns the phase coherence is lost. We want to clarify the nature of these subtle chaotic bifurcations (i.e., the process of phase decoherence), and whether these bifurcations are characterized by abrupt or continuous changes.

We integrate Eq. (6) with a fourth-order Runge-Kutta method and a time step of 0.05, by incrementing the parameter a from 0.15 to 0.30 by 1.25×10^{-6} at each integration step. This gives a data set $x(t)$ of total length 120 001 points. We use our Algorithm 1 to study $x(t)$. We compute $\overline{T_2}(r)$ on time series $x(t)$ data within episodic windows consisting of 2000 consecutive points. Sequential windows are shifted by 10 points (thus overlapping by 1990 points), giving a total of 11 801 values for $\overline{T_2}(r)$. The result is shown in Fig. 10 as the very irregular upper curve. For the parameter range shown, the curve suggests three periodic windows, as indicated by arrows and denoted by capital letters *A*, *B*, and *C* in the figure. By integrating Eq. (6) with fixed a belonging to those windows, we find that motions corresponding to those parameter values are indeed periodic. The existence of those periodic windows has two important implications: (i) The development of the funnel [Figs. 9(b) and 9(c), especially 9(d)] does not follow directly from the simple Rossler attractor [Fig. 9(a)], since these states are separated by periodic windows and (ii) phase decoherence has to really refer to the variation of chaotic behavior for a belonging to the second chaotic window, roughly [0.17, 0.24]. This result also compels us to think more carefully what characterizes phase decoherence.

A sharp peak in a power spectrum can be generated by two mechanisms: a perfect periodic signal or a signal with fixed frequency but varying amplitude. Phase decoherence here refers to the latter case. For example, if one computes the time elapse between successive maxima of the chaotic signal $x(t)$ corresponding to $a=0.17$, then one finds that this period is almost a constant. This suggests that we consider the following time series: $\theta(t)=\arctan[x(t+L)/x(t)]$, where L is chosen to be 15 sampling time interval here. With this L, the phase diagram, $x(t+L)$ vs $x(t)$, looks similar to those of Fig. 9. We then compute $\overline{T_2}(r)$ from $\theta(t)$. The result is shown in Fig. 10 as the much regular lower curve. Very interestingly, the curve also suggests a periodic window that is identical to the window *C* given by $x(t)$. In order to examine this curve more clearly, we magnify the segment for $a\in[0.15,0.24]$ and replot it as Fig. 11. We find that for a smaller than 0.177, so long as the phase information is concerned, the chaotic motion (for example, $a=0.15$ and 0.17)

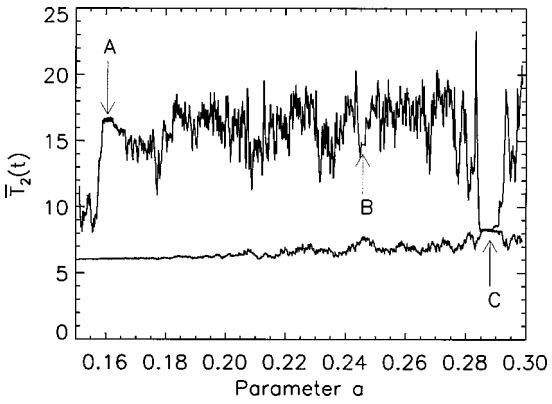

FIG. 10. Variation of $\bar{T}_2(r)$ with the parameter a for $x(t)$ (upper irregular curve) and $\theta(t)$ (lower more regular curve). The embedding parameters are $m=3$ and $L=10$. The scale r used is 2^{-4}.

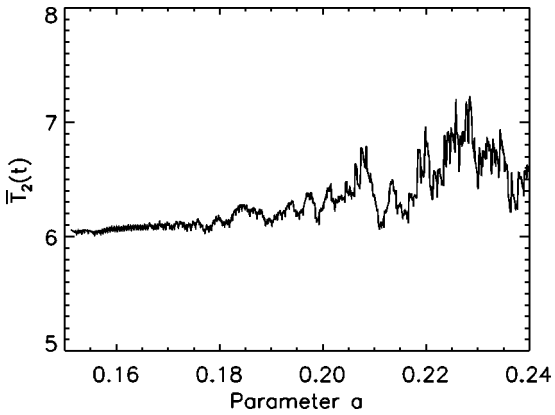

FIG. 11. A magnification of part of the lower more regular curve of Fig. 10.

and the periodic motion (for example, $a=0.16$) are not much different, since $\bar{T}_2(r)$ varies only slightly. The transition starts around $a=0.18$, and becomes more dramatic around $a=0.20$. Overall, however, the changes are gradual rather than abrupt. These quantitative features are consistent with those qualitative ones obtained by visually inspecting the phase diagrams and PSD's of Fig. 9.

As in the transient Lorenz system, we have also observed that similar results are obtained when different embedding parameters and scales r are used, and when the size of the data subset is 1000 points.

V. CONCLUSIONS

In this paper, we have analyzed a number of interesting dynamical systems to detect nonstationarity and transience in time series, and to understand various consequences of nonstationarity. In particular, we find that nonstationarity in the metastable chaotic Lorenz system is due to nonrecurrence. Nonrecurrence then determines lack of fractal structure in the signal. In $1/f^{\alpha}$ noise, we find that the correlation dimension associated with such noisy processes are local graph dimensions calculated from sojourn points. While the presence of such dimensions has been considered one of the pitfalls of the Grassberger-Procaccia algorithm, we have argued that being able to readily estimate the key parameter for $1/f^{\alpha}$ noise should actually be regarded as a merit of the algorithm, so long as the danger of interpreting $1/f^{\alpha}$ noise as deterministic chaos is absent.

We have also designed a transient Lorenz system with a slowly oscillating controlling parameter, and a transient Rossler system with a slowly linearly increasing parameter, with the parameter range covering a sequence of chaotic dynamics with increased phase incoherence. State transitions, from periodic to chaotic, and vice versa, have been identified, together with different facets of nonstationarity in each phase. These results do not depend sensitively on the specific values for the embedding parameters, the size of the ball, and the length of the data subset, indicating the method should be easy to use in practice.

While the main purpose of this paper is to detect state transitions in experimental situations, the techniques may also be used to detect the bifurcations of a system when the equations of motion are known. More precisely, when many parameters are involved, one may integrate or iterate the equations of motion by continuously varying one or a few parameters in every time step, and then study how the features of the motion change with time [hence, parameter(s)].

ACKNOWLEDGMENTS

The author thanks Johnny Lin for proofreading the manuscript and correcting the English.

[1] A. Provenzale, A. R. Osborne, and R. Soj, Physica D **47**, 361 (1991).
[2] A. R. Osborne and A. Provenzale, Physica D **35**, 357 (1989); J. Theiler, Phys. Lett. A **155**, 480 (1991).
[3] J. P. Eckmann, S. O. Kamphorst, and D. Ruelle, Europhys. Lett. **4**, 973 (1987).
[4] L. L. Trulla, A. Giuliant, J. P. Zbilut, and C. L. Webber, Phys. Lett. A **223**, 255 (1996).
[5] A. Provenzale, L. A. Smith, R. Vio, and G. Murante, Physica D **58**, 31 (1992).
[6] D. J. Yu, W. P. Lu, and R. G. Harrison, Phys. Lett. A **250**, 323 (1998); Chaos **9**, 865 (1999).
[7] R. Manuca and R. Savit, Physica D **99**, 134 (1996).
[8] M. B. Kennel, Phys. Rev. E **56**, 316 (1997).
[9] H. Kantz, Phys. Rev. E **49**, 5091 (1994).
[10] T. Schreiber, Phys. Rev. Lett. **78**, 843 (1997).
[11] J. B. Gao, Phys. Rev. Lett. **83**, 3178 (1999).
[12] D. Farmer, J. Crutchfield, H. Froehling, N. Pachard, and R. Shaw, Ann. N.Y. Acad. Sci. **357**, 453 (1980).
[13] J. S. Iwanski and E. Bradley, Chaos **8**, 861 (1998).
[14] J. B. Gao and H. Q. Cai, Phys. Lett. A **270**, 75 (2000).
[15] N. H. Packard, J. P. Crutchfield, J. D. Farmer, and R. S. Shaw, Phys. Rev. Lett. **45**, 712 (1980); F. Takens, in *Dynamical Systems and Turbulence*, Lecture Notes in Mathematics Vol. 898,

edited by D. A. Rand and L. S. Young (Springer-Verlag, Berlin, 1981), p. 366.
[16] J. A. Yorke and E. D. Yorke, J. Stat. Phys. **21**, 263 (1979).
[17] E. Ott, *Chaos in Dynamical Systems* (Cambridge University Press, Cambridge, 1993).
[18] J. L. Kaplan and J. A. Yorke, Commun. Math. Phys. **67**, 93 (1979).
[19] P. Grassberger and P. Procaccia, Phys. Rev. Lett. **50**, 346 (1983).
[20] W. H. Press, Comments. Astrophys. **7**, 103 (1978).
[21] P. Bak, *How Nature Works: The Science of Self-Organized Criticality* (Copernicus, NY, 1996).
[22] A. Davis, A. Marshak, W. Wiscombe, and R. Cahalan, J. Geophys. Res. **99**, 8055 (1994); also in *Current Topics in Nonstationary Analysis*, edited by G. Trevilo, J. Hardin, B. Douglas, and E. Andreas (World Scientific, Singapore, 1996), pp. 97–158.
[23] O. E. Rossler, Ann. N.Y. Acad. Sci. **316**, 376 (1978).